Reduced Glutamate Decarboxylase 65 Protein within Primary Auditory Cortex Inhibitory Boutons in Schizophrenia

Supplemental Information

Supplemental Methods

Subjects

All of the brain specimens were collected during autopsies conducted at the Allegheny County Medical Examiner's Office, with permission obtained from the subjects' next-of-kin. The protocol used to obtain consent was approved by the University of Pittsburgh Institutional Review Board and Committee for Oversight of Research Involving the Dead. An independent committee of experienced clinicians made consensus diagnoses (1) for each subject, using information obtained from clinical records and structured interviews with surviving relatives. These procedures were IRB approved.

Cohort 1 Tissue Processing

Brains from individuals in cohort 1 were bisected and the left hemisphere of each subject was cut coronally into 1-2 cm-thick blocks, which were then immersed in cold 4% paraformaldehyde in phosphate buffer for 48 hours, equilibrated in a series of graded sucrose solutions, and stored at -30^{o}C in an antifreeze solution (30% glycerol and 30% ethylene glycol in phosphate-buffered saline). Superior temporal gyrus (STG)-containing blocks were generated as described previously (2,3) and 40 µm coronal cryostat sections were cut and then stored in antifreeze solution at -30^{o}C until use in this study.

Cohort 2 Tissue Processing

Brain specimens from individuals in cohort 2 were harvested, bisected, blocked coronally, and stored in antifreeze solution at -30^{o}C as described for cohort 1 (4,5). The entirety of the left STG of each subject was dissected from the fixed coronal blocks. The pial surfaces of the STG blocks were painted with hematoxylin to facilitate identification of the pial surface later during tissue processing, and the blocks were reassembled in 7% low melting point agarose in their *in vivo* orientation. The reassembled STG was cut into systematic uniformly random 3 mm slabs orthogonal to the long axis of Heschl's gyrus. Every other slab with a random start was selected for mapping the boundaries of primary auditory cortex and the remaining slabs were stored in antifreeze solution until use. Mapping slabs were cut on a

cryostat at 60 µm, and three consecutive sections from each slab were stained for parvalbumin (PV) immunoreactivity, acetylcholinesterase activity, and Nissl substance. These sections were used to determine whether primary auditory cortex was present in a given slab, to estimate the volume of primary auditory cortex, and to delineate the boundaries of primary auditory cortex. The boundaries of primary auditory cortex determined using the mapping slabs were applied to the unused set of slabs, such that boundaries of primary auditory cortex on a mapping slab were applied to the adjacent unused slab immediately rostral. The primary auditory cortex was dissected from the unused slabs, and further subdivided into 3 mm wide blocks. Blocks from the most rostral and caudal slabs containing the region of interest were weighted at 1/3 relative to the weight of other blocks to account for the fact that these blocks only partially contained the region of interest. This weighting method has been previously published (4). Briefly, it is needed because the end blocks only partially represent the region of interest (on average less than half due to the positive curvature of the boundary of the region of interest in 3 dimensions) and therefore should not have the same weight as the other blocks. However, there is no way to know the precise weight without knowing the exact fraction of the region of interest and the Nv of the region of interest as well as that of the neighboring region within each block in question. Because the positive curvature is best approximated by a cone or a pyramid, it would take up 1/3 of the volume, leading to our weighting. Block weights were factored into calculations of bouton number (4). Each primary auditory cortex block was then placed pial surface down in a layer of optimal cutting temperature compound (OCT) on a stainless steel block. A hollow cylinder was placed on the block over the tissue, and the cylinder was filled with OCT and allowed to freeze at -20^{o}C. The block of tissue encased in OCT was then removed from the cylinder and placed in a stainless steel well where it was randomly rotated and fixed in its orientation with OCT. The primary auditory cortex block was then sectioned at 50 µm in this orientation perpendicular to the pial surface, and sections were stored at -30^{o}C in antifreeze solution until use in this study

Antipsychotic-exposed Macaque Cohort Tissue Processing

In order to account for possible effects of antipsychotic medications, we studied a previously described cohort (6) of four male macaque monkeys (*Macaca fascicularis*) chronically exposed to haloperidol decanoate, and four control macaques matched for sex and weight. All procedures were approved by the University of Pittsburgh's Institutional Animal Care and Use Committee. Animals received injections of haloperidol (mean (standard deviation) = 16.0 (2.1) mg/kg) every four weeks, maintaining trough serum levels of haloperidol of 4.3 (1.1)

ng/ml, on average. Following 9-12 months of haloperidol exposure, animals were euthanized with an overdose of pentobarbital, and brains were removed and immersed in 4% paraformaldehyde following a 45 minute post mortem interval (PMI). Free-floating sections from the four matched pairs were processed together within immunohistochemistry runs, and procedures were identical to those described for human tissue immunohistochemistry.

Immunohistochemistry

In order to identify axon boutons of inhibitory gamma-aminobutyric acid (GABA)ergic neurons in the primary auditory cortex, we utilized an antibody directed against GAD65. GAD65 is highly expressed in GABAergic boutons, with minimal expression in interneuron cell bodies (7). The antibody we selected (mouse anti-GAD65 monoclonal, Millipore, MAB351) is a clone of the monoclonal GAD-6 antibody developed by Chang and Gottlieb that recognizes only the lower molecular weight band of GAD in Western blots (8). We have verified this by Western blot, and also found that this antibody does not label brain homogenate from GAD65 knockout mice (Figure S1A). In immunohistochemistry, labeling with this antibody has been reported to colocalize with punctate structures immunoreactive for GAD67, cannabinoid receptor 1 (CB1) and PV (presumably inhibitory boutons) (9), and in immunoelectron microscopy has been reported to label symmetrical synapses (10), as well as punctate structures closely apposed to puncta immunoreactive for the α1 subunit of the $GABA_A$ receptor (11). Qualitatively, we observed no colocalization of puncta labeled with the GAD65 antibody and antibodies against vesicular glutamate transporters (VGLUT1 and VGLUT2), which label intracortical and thalamocortical excitatory boutons, respectively (Figure S1B). In summary, this evidence suggests that this antibody is specific for GAD65, and in immunohistochemistry is specific for non-glutamatergic boutons and labels structures colocalized with or closely apposed to other GABAergic synaptic markers.

Auditory cortex containing tissue sections from matched pairs were processed together in immunohistochemistry runs. Free-floating sections were rinsed in 0.1 M phosphate buffered saline (PBS), and then incubated in 1% $NaBH_4$ in phosphate buffer for 30 minutes to reduce tissue autofluorescence. Sections were rinsed again in PBS and incubated for 3 hours in blocking buffer containing 0.3% Triton-X, 5% normal human serum, 5% normal goat serum, 1% bovine serum albumin, 0.1% lysine, and 0.1% glycine in PBS. Sections were then incubated with a 1:500 dilution of anti-GAD65 primary antibody (MAB351) in blocking buffer for 96 hours at 4^oC. After rinsing in PBS, sections were incubated overnight with a 1:500 dilution of Alexa 405 goat anti-mouse secondary antibody (Invitrogen, Carlsbad, CA). Sections were rinsed, mounted

on gelatin-coated slides, allowed to dry for 1 hour, rehydrated for 10 minutes in distilled water, and coverslipped with Vectashield Hard Set mounting medium (Vector Laboratories, Burlingame, CA).

Image Collection

Images were collected using a 1.42 NA 60X oil objective on an Olympus BX51 upright microscope (Olympus, Center Valley, PA) equipped with an Olympus DSU spinning disk confocal, a Hamamatsu C4742-98 CCD camera (Hamamatsu, Bridgewater, NJ), Olympus mercury light source, excitation/emission filter wheels, a 89000 Sedat Quad ET filter set (Chroma Technology Corp, Bellows Falls, VT), and high precision Prior Scientific motorized XY stage (Prior Scientific, Inc., Rockland, MD) equipped with a linear XYZ encoder (Ludl Electronic Products, Ltd., Hawthorne, NY). Image collection was controlled using SlideBook version 4.1 software (Intelligent Imaging Innovations, Denver, CO). At each sampling site, the tissue thickness (Z axis depth) was measured and recorded, and tissue thickness did not differ between diagnostic groups (t_{52} = 0.844, p = 0.402). Image stacks were collected with a step size of 0.22 µm between Z axis planes in the stack, starting from 10 µm below the tissue surface closest to the coverglass and stepping up until the tissue surface was reached, yielding a 10 µm thick (Z axis depth) stack comprised of 46 individual 2-dimensional planes. Collected image planes were 512 x 512 pixels with 2 x 2 binning, and exposure times were adjusted to optimize the spread of the intensity histogram and to ensure that none of the pixels in the image stack were saturated. Although mean exposure time was not significantly different between diagnostic groups (Means: Control, 1643 ms; Schizophrenia, 1796 ms; t_{52} = 0.45, p = 0.654), differences were corrected for by including exposure times in statistical models.

Image Processing

Collected image stacks were post-processed offline, using SlideBook and Automation Anywhere software (Automation Anywhere, Inc., San Jose, CA) to automate keystrokes and increase image processing efficiency. Images were deconvolved with a constrained iterative algorithm using a calculated point spread function, a maximum of 20 iterations, 3D frequency filtering enabled, and Gaussian noise smoothing with a radius of 0.5. The background fluorescence intensity of each smoothed and deconvolved image stack was determined as the mode value of the intensity histogram. Background subtraction was done by subtracting the mode intensity (gray scale) value from all pixel intensities in the image stack. This deconvolved, smoothed, and background subtracted image stack was then subject to intensity segmentation

coupled with morphological selection using our iterative masking approach (12). For each image stack, the initial intensity threshold was set at 105% of the background intensity level determined above, and with each subsequent iteration the intensity threshold was increased by 10%, until either a maximum of 5000 gray levels was reached or a maximum of 60 iterations occurred. After each segmentation step, mask objects with volumes ranging from 0.06 μm^3 to 1.0 μm^3 were selected and merged with the mask generated in the prior segmentation step. The resulting mask was then copied back onto the original image stack which had been deconvolved as described above, but without the Gaussian smoothing step, in order to obtain accurate pixel intensity information. GAD65-immunoreactive (IR) bouton data (mean intensity, mean volume) were extracted from these image stacks using the generated mask to identify objects of interest. Mask objects were selected for final analysis if the intensity gray level range within the object (maximum voxel intensity minus minimum voxel intensity) was greater than 50. This further eliminated falsely detected background signal, as objects identified from background noise are likely to have less intensity variation between highest and lowest intensity gray scale pixels. GAD65-IR puncta were counted automatically by determining whether the centroid of each automatically detected object was inside the disector. This corresponds to the so-called "associated point rule" (ref. 13, page 69), which is an unbiased alternative to the unbiased counting frame (14). Guard zones of 10 pixels were applied around all edges in the X and Y dimensions of each stack, and 10 Z planes starting 10 planes below the coverglass were included in analysis, as antibody penetration was uniform (puncta counts and intensities were uniform) across these Z axis depths (10 planes x 0.22 μm step size = 2.20 μm disector height).

Calculation of GAD65-IR Bouton Density and Number

Densities reported in Figure 3 were calculated individually at each site in order to include exposure time as a covariate in our analyses, as exposure time varied on a site-by-site basis. The density of mask objects at each site was determined by dividing the number of objects counted at each site by the product of the disector height (2.2 μm) and the area of the counting frame (2553 μm^2), and then multiplying that by the measured tissue thickness at each site divided by the cryostat block advance (40 μm (cohort 1) or 50 μm (cohort 2)) (15) to correct for tissue shrinkage. It should be noted that the disector height of 2.2 μm used in the current study is very low and could only be implemented robustly because we used confocal microscopy allowing for a high number of thin focal planes; and because we performed a careful analysis of the distribution of the boutons along the Z axis (see Fig. 4 of (16)). We determined the position of the disector and corresponding guard zones *post hoc* ensuring that boutons were only

sampled in the zone with uniform bouton counts. Such sampling was possible due to the high number of automatically detected boutons—on average 23,037 boutons were detected per subject and of these an average of 5,742 per subject were sampled by the disector. Thus, while a disector height of only 2.2 μm should be avoided in a standard brightfield microscopy study with manual counts, we were able to robustly implement such a disector in the current study.

For cohort 2 subjects, we were also able to estimate GAD65-IR bouton number because of the tissue processing methods used to generate auditory cortex tissue sections. To do this, mean object densities were calculated as described in equations 4 and 5 of Dorph-Petersen *et al.* 2009 (4) using the numerical density (N_V) approach with the following modification: the distances of each individual mask object from the central axis were not included in the calculation under the reasonably robust assumption of homogeneity on the scale of the sampling site (~50 μm). Instead, object counts at each sampling site were weighted by multiplying object count at each site by the distance of the sampling site from the central axis. Deep layer 3 volumes for each subject were calculated as described in equations 1-3 of Dorph-Petersen *et al.* (4) by multiplying the volume fraction of deep layer 3 sampled by the total primary auditory cortex volume. Bouton number for each subject was then generated by multiplying the N_V by the total deep layer 3 volume (equation 6 from (4)).

Statistical Analyses

For each human and macaque subject, mean density, fluorescence intensity, and volume of GAD65-IR puncta in deep layer 3 of primary auditory cortex were calculated. Among the human subjects, the analyses of GAD65-IR bouton volume, density, and mean intensity were conducted separately using two multivariate analysis of covariance (MANCOVA) models: a primary model that included diagnosis and cohort as fixed effects, subject pair (nested in cohort) as a blocking factor, and tissue storage time and exposure time as covariates; and a secondary model without subject pair as a blocking factor, that included diagnosis, sex, and cohort as fixed effects and age, PMI, tissue storage time, and exposure time as covariates. To help satisfy the normality requirement for MANCOVA models, mean fluorescence intensity was analyzed on the natural logarithm scale. To account for the correlation among sampling sites within each subject and among sampling sites within each section for each subject, site and section nested in subject were included as random effects in each MANCOVA model. Inclusion of tissue thickness, subject handedness, or immunohistochemistry assay order in the models had negligible impact on diagnostic group differences and, thus, the results reported are from MANCOVA models omitting these factors.

The analysis of GAD65-IR bouton number (cohort 2 subjects only) was conducted using two analysis of covariance (ANCOVA) models: a primary model that included diagnosis and pair as fixed effects, and tissue storage time as a covariate; and a secondary model without pair as a factor that included diagnosis and sex as fixed effects, and age, PMI, and tissue storage time as covariates. Correlations between dendritic spine density and GAD65-IR bouton fluorescence intensity or density for cohort 1 subjects (as spine density measures were not available for cohort 2 subjects) (17) were assessed using Pearson's correlation.

Based on the mean densities, fluorescence intensities, and volumes for each subject, two sample *t* tests were used to determine the effect of the following: antipsychotic use, co-morbid alcohol or substance abuse, independent living status at time of death, history of cannabis use, death by suicide, diagnosis of schizoaffective disorder, and benzodiazepine, antidepressant, or anticonvulsant medication status at time of death. In these analyses, the percent changes of bouton density, fluorescence intensity, and volume in subjects with schizophrenia (relative to normal controls) within each subject pair were the response variables of interest.

To compare mean bouton density, fluorescence intensity, and volume between antipsychotic exposed and control macaques, MANCOVA models were used, each of which included drug treatment as a fixed effect, pair as a blocking factor, and exposure time as a covariate, and site and section nested in animal were included as random effects. Due to the similarity of storage time within each pair, storage time was not included as a covariate.

All statistical tests were two-sided and conducted at the 0.05 significance level.

Supplemental Results

Clinical Factors

We tested for associations between pair-wise changes in GAD65-IR mean bouton density, fluorescence intensity, and volume and a number of clinical confounds including: whether the subject had a diagnosis of schizophrenia or schizoaffective disorder, died by suicide, had a history of alcohol or other substance abuse, or was on or off antipsychotics, anticonvulsants, or benzodiazepines at time of death (Figure S2). We found a significant relationship between benzodiazepine use at time of death and percent change in GAD65-IR bouton density ($t_{23} = 2.64$, $p = 0.015$). The mean (95% confidence interval) percent change in bouton density for subject pairs in which the schizophrenia subject was taking benzodiazepines

at time of death was a 17.7% (3.3%, 32.0%) increase relative to normal controls, and a 2.7% (-4.6%, 10%) decrease for subject pairs in which the schizophrenia subject was not taking benzodiazepines at time of death. Additionally, we determined that there was no effect of subjects' history of cannabis use or antidepressant use at time of death on the percent change in GAD65-IR mean bouton density, fluorescence intensity, or volume (data not shown; *Cannabis*: Intensity, $t_{22} = 0.06$, $p = 0.953$; Density, $t_{22} = 0.42$, $p = 0.677$; Volume, $t_{22} = 0.72$, $p = 0.481$; *Antidepressants*: Intensity, $t_{24} = -0.4$, $p = 0.692$; Density, $t_{24} = -0.22$, $p = 0.829$; Volume, $t_{24} = -1.52$, $p = 0.140$).

Supplemental Discussion

Clinical Factors

GAD65-IR bouton fluorescence intensity, density, and volume did not differ between schizophrenia subjects who were on or off antipsychotic medication at time of death, or between monkeys chronically exposed to haloperidol and control monkeys. This suggests that the reduction in GAD65-IR bouton fluorescence intensity observed in subjects with schizophrenia is not an effect of antipsychotic medications. On the contrary, use of antipsychotic medications in our subjects may actually result in underestimation of the effect of disease on GAD65 fluorescence intensities, as we observed a non-significant trend toward increased GAD65-IR bouton fluorescence intensity in the antipsychotic exposed monkeys.

A number of our subjects were taking benzodiazepines, antidepressants, or anticonvulsant medications at time of death (see Table S1). Because of the potential impact of these medications on the GABAergic system (18, reviewed in (19,20)) we tested for significant effects of their use at time of death. We did not find any significant effects of benzodiazepines, anticonvulsants, or antidepressants on the fluorescence intensity of GAD65-IR boutons. From this, we conclude that our finding of decreased within-bouton GAD65 protein is not caused by exposure to these medications. However, we found that schizophrenia subjects who were on benzodiazepines at time of death had a significantly larger percent increase (relative to controls) in the density of GAD65-IR boutons compared to schizophrenia subjects who were not on benzodiazepines at time of death, who actually had a percent decrease. This association could indicate that benzodiazepines increase the density of GAD65-IR boutons, or that those subjects with greater GAD65-IR bouton density are more likely to be treated with benzodiazepines; however, the most probable interpretation is that benzodiazepine exposure leads to a non-

significant increase in GAD65 protein levels within boutons, causing us to detect more GAD65-IR boutons in schizophrenia subjects who were taking benzodiazepines at time of death. In support of this, chronic benzodiazepine exposure increases GAD65 mRNA (21), and our data trend toward increased GAD65-IR bouton fluorescence intensity in subjects on benzodiazepines at time of death (Figure S2).

Table S1. Characteristics of control subjects and subjects with schizophrenia in cohort 1 (top, green) and cohort 2 (bottom, blue). S/R/A, sex/race/age; PMI, postmortem interval; Hand, handedness; Meds ATOD, medications used at time of death; ASCVD, atherosclerotic coronary vascular disease; AAC, alcohol abuse, current at time of death; AAR, alcohol abuse, in remission at time of death; ADC, alcohol dependence, current at time of death; ADR, alcohol dependence, in remission at time of death; OAC, other substance abuse, current at time of death; OAR, other substance abuse, in remission at time of death; ODC, other substance dependence, current at time of death; ODR, other substance dependence, in remission at time of death; L, left; M, mixed; R, right; U, unknown; B, benzodiazepines; C, anticonvulsants; D, antidepressants; L, lithium; N, no medications; O, other medication(s); P, antipsychotic; *Control subject 396 tested positive for benzodiazepines at autopsy. **Control subject 987 diagnosed with post traumatic stress disorder- in remission 39 years.

Control Subjects							Schizophrenia Subjects								
Pair	Case	S/R/A	Hand	PMI (h)	Storage Time (mos)	Cause of Death	Case	S/R/A	Hand	PMI (h)	Storage Time (mos)	Cause of Death	Diagnosis	Cannabis History	Living Independently ATOD	Meds ATOD
Cohort 1																
1	250	F/W/47	R	5.3	211.2	ASCVD	398	F/W/41	U	10.3	166.9	Pulmonary embolism	Schizoaffective disorder	unknown	no	B,C,O,P
2	620	M/W/64	R	17.3	139.3	Accidental drowning	566	M/W/63	R	18.3	148.7	ASCVD	Chronic undifferentiated schizophrenia, AAR	no	no	B,D,O,P
3	681	M/W/51	R	11.6	131.6	Hypertrophic cardiomyopathy	234	M/W/51	R	12.8	214.1	Cardiomyopathy	Chronic paranoid schizophrenia	no	yes	N
4	643	M/W/50	R	24	136.4	ASCVD	581	M/W/46	A	28.1	146.3	Accidental combined drug overdose	Chronic paranoid schizophrenia, ADC, OAC	yes	yes	B,C,O,P
5	634	M/W/52	L	16.2	137.5	ASCVD	625	M/B/49	R	23.5	138.7	ASCVD	Chronic disorganized schizophrenia, AAC	no	no	D,O,P
6	474	F/B/49	U	13.4	166.8	Hypertensive cardiovascular disease	656	F/B/47	R	20.1	134.9	Suicide by gun shot	Schizoaffective disorder, ADC	no	yes	O,P,V
7	396*	M/W/41	L	17.5	167.1	ASCVD	408	M/W/46	R	19.8	185.5	ASCVD	Chronic paranoid schizophrenia	no	yes	B,D,O,P
8	449	F/W/47	L	4.3	170.3	Accidental CO poisoning	517	F/W/48	R	3.7	155.7	Intracerebral hemorrhage	Chronic disorganized schizophrenia, ADC	no	no	C,P
9	451	M/W/48	L	12	170.0	ASCVD	317	M/W/48	U	8.3	201.4	Bronchopneumonia	Chronic undifferentiated schizophrenia	no	no	D,O,P
10	178	M/W/48	R	7.8	221.9	ASCVD	377	M/W/52	R	10.0	192.7	GI bleeding	Chronic undifferentiated schizophrenia, ADC	no	yes	O,P
11	412	M/W/42	R	14.2	184.5	Aortic stenosis	466	M/B/48	U	19.0	168.0	ASCVD	Chronic undifferentiated schizophrenia	unknown	no	O,P
12	285	F/W/27	R	16.5	206.6	Trauma	587	F/B/38	R	17.8	144.9	Myocardial hypertrophy	Chronic undifferentiated schizophrenia, AAR	yes	no	B,O,P,V
13	575	F/B/55	R	11.3	146.8	ASCVD	597	F/W/46	L	10.1	143.4	Pneumonia	Schizoaffective disorder	no	yes	D,O,P
14	592	M/B/41	R	22.1	144.1	ASCVD	450	M/B/48	L	22.0	170.2	Suicide by jumping	Chronic undifferentiated schizophrenia, ADR, ODR	yes	no	N
15	452	F/W/40	R	14.3	169.9	ASCVD	341	F/W/47	L	14.5	198.8	Suicide by drug overdose	Chronic undifferentiated schizophrenia, AAC	no	yes	O,P
Cohort 2																
1	700	M/W/42	R	26.1	131.6	ASCVD	533	M/W/40	R	29.1	156.7	Accidental asphyxiation	Chronic undifferentiated schizophrenia	no	no	P
2	806	M/W/57	R	24.0	113.1	Pulmonary thromboembolism	665	M/B/59	R	28.1	137.2	Intestinal hemorrhage	Chronic paranoid schizophrenia, ADC	no	yes	D,O,P
3	739	M/W/40	R	15.8	126.6	ASCVD	1088	M/W/49	R	21.5	63.1	Accidental combined drug toxicity	Unidfferentiated schizophrenia, ADC, OAC	yes	no	D,O,P
4	822	M/B/28	L	25.3	110.5	ASCVD	787	M/B/27	L	19.2	116.7	Suicide by gunshot to head	Schizoaffective disorder, ODC	yes	no	O,P
5	727	M/B/19	R	7.0	127.5	Trauma	829	M/W/25	U	5.0	108.4	Suicide by salicylate overdose	Schizoaffective disorder, ADC, OAR	yes	no	B,C
6	659	M/O/46	R	22.3	137.9	Peritonitis	930	M/W/47	R	15.7	88.2	ASCVD	Continuous disorganized schizophrenia, ADR, OAR	yes	no	C,O,P
7	1047	M/W/43	R	12.4	69.3	ASCVD	933	M/W/44	U	8.3	87.6	Myocarditis	Disorganized schizophrenia	no	no	C,D,O,P
8	852	M/W/54	R	8.0	102.9	Cardiac tamponade	722	M/B/45	R	9.1	128.0	Upper GI bleed	Undifferentiated schizophrenia, ODR, OAR	yes	no	B,O,P
9	685	M/W/56	R	14.5	134.0	Hypoplastic coronary artery disease	1105	M/W/53	R	7.9	61.2	ASCVD	Schizoaffective disorder	no	no	P
10	686	F/W/52	R	22.6	133.7	ASCVD	802	F/W/63	A	29.0	113.7	Right ventricular dysplasia	Schizoaffective disorder, ADC, ODR	no	yes	C,O,P
11	987**	F/W/65	R	21.5	78.5	ASCVD	917	F/W/71	U	23.8	91.6	ASCVD	Chronic Unidfferentiated schizophrenia	no	no	O,P
12	1092	F/B/39	R	16.6	62.7	Mitral valve prolapse	1010	F/B/44	L	18.7	75.4	Sudden unexpected death in epilepsy	Chronic Undifferentiated schizophrenia, MMR	no	no	C,D,P

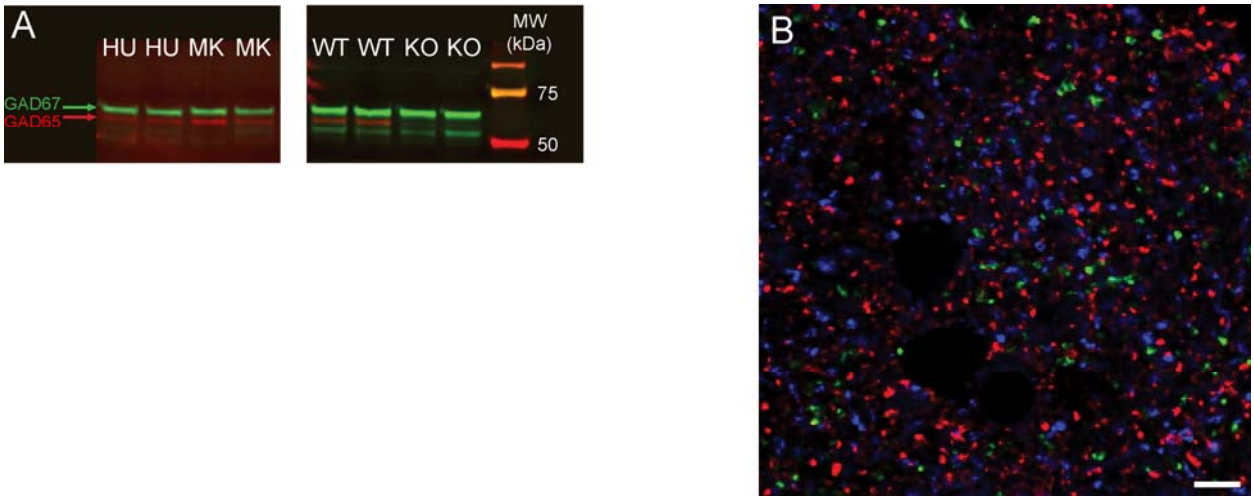

Figure S1. Specificity of GAD65 antibody. (**A**) Western blot demonstrating labeling with mouse anti-GAD65 monoclonal antibody (Millipore) (red) showing specificity for the lower molecular weight isoform of GAD in human (HU) and monkey (MK). To demonstrate antibody specificity for the 65 kDa isoform, blots were labeled with rabbit anti-GAD67 antibody (Sigma-Aldrich) (green). Red channel intensity is shown increased for visualization purposes on left half of blot. Right half of blot shows GAD65 antibody labeling in wild type (WT) and GAD65-knockout (KO) mouse cortical gray matter. GAD65 immunoreactivity is absent in the GAD65-KO tissue, as expected. (**B**) Human auditory cortex labeled with the GAD65 antibody (blue), as well as antibodies against vesicular glutamate transporters, VGLUT1 (red) and VGLUT2 (green), to label intracortical and thalamocortical glutamatergic boutons, respectively. Projection image was processed with background subtraction and constrained iterative deconvolution (see Methods and Materials). No colocalization is observed between GAD65 antibody and excitatory bouton markers. Scale bar is 10 µm.

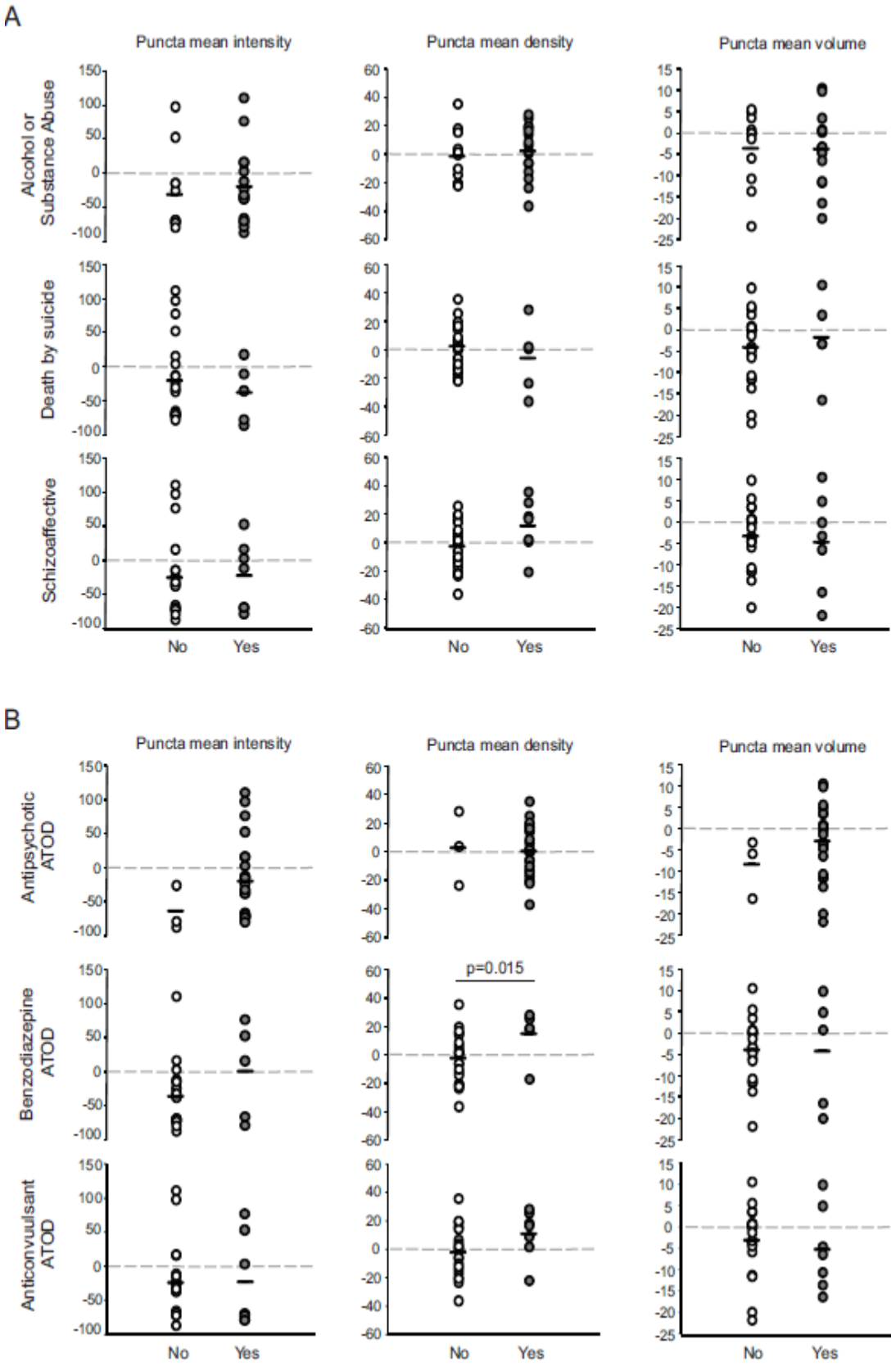
A
Puncta mean intensity
Puncta mean density
Puncta mean volume
Alcohol or Substance Abuse
Death by suicide
Schizoaffective
No
Yes
B
Puncta mean intensity
Puncta mean density
Puncta mean volume
Antipsychotic ATOD
Benzodiazepine ATOD
Anticonvuulsant ATOD
p=0.015
No
Yes

Figure S2. Percent change in GAD65-immunoreactive (IR) puncta features associated with schizophrenia subject clinical features and medication status at time of death. (**A**) Percent change in GAD65-IR puncta fluorescence intensity *(left)*, density *(middle)* and volume *(right)* as a function of history of alcohol or substance abuse, death by suicide or diagnosis of schizoaffective disorder. (**B**) Percent change in GAD65-IR puncta fluorescence intensity *(left)*, density *(middle)* and volume *(right)* as a function of current antipsychotic use at time of death, benzodiazepine use at time of death, or anticonvulsant drug use at time of death (ATOD). Dotted line at 0% indicates no difference between schizophrenia and control subject. Horizontal bars indicate group means.

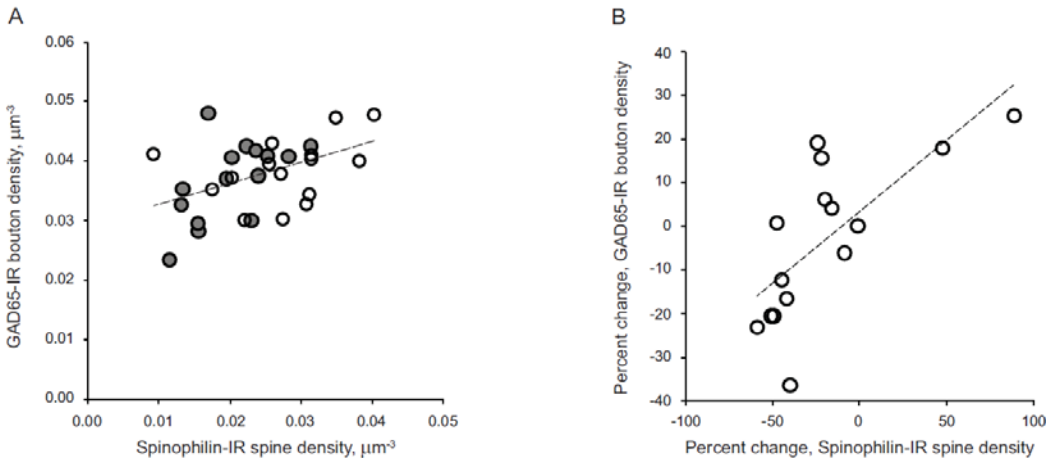

Figure S3. Correlations between mean and percent change in GAD65-immunoreactive (IR) puncta density and spine density in primary auditory cortex. (**A**) Mean GAD65-IR puncta density plotted as a function of spinophilin-IR puncta density for each subject in cohort 1. Open circles = control, filled circles = schizophrenia. Dashed line represents the regression line (Pearson $r = 0.457$, $p = 0.01$). (**B**) The percent change in GAD65-IR puncta density plotted as a function of the percent change in spinophilin-IR puncta density for pairs in cohort 1 (schizophrenia subjects relative to matched controls). Dashed line represents the regression line (Pearson $r = 0.718$, $p = 0.003$).

Supplemental References

1. American Psychiatric Association (1994): *Diagnostic and Statistical Manual of Mental Disorders, 4th ed*. American Psychiatric Press, Washington, D.C..

2. Sweet RA, Pierri JN, Auh S, Sampson AR, Lewis DA (2003): Reduced pyramidal cell somal volume in auditory association cortex of subjects with schizophrenia. *Neuropsychopharmacology* 28:599-609.

3. Sweet RA, Bergen SE, Sun Z, Sampson AR, Pierri JN, Lewis DA (2004): Pyramidal cell size reduction in schizophrenia: evidence for involvement of auditory feedforward circuits. *Biol Psychiatry* 55:1128-1137.

4. Dorph-Petersen K-A, Delevich KM, Marcsisin MJ, Zhang W, Sampson AR, Gundersen HJ, *et al.* (2009): Pyramidal neuron number in layer 3 of primary auditory cortex of subjects with schizophrenia. *Brain Res* 1285:42-57.

5. Sweet RA, Dorph-Petersen K-A, Lewis DA (2005): Mapping auditory core, lateral belt, and parabelt cortices in the human superior temporal gyrus. *J Comp Neurol* 491:270-289.

6. Sweet RA, Bergen SE, Sun Z, Marcsisin MJ, Sampson AR, Lewis DA (2007): Anatomical evidence of impaired feedforward auditory processing in schizophrenia. *Biol Psychiatry* 61:854-864.

7. Erlander MG, Tillakaratne NJ, Feldblum S, Patel N, Tobin AJ (1991): Two genes encode distinct glutamate decarboxylases. *Neuron* 7:91-100.

8. Chang YC, Gottlieb DI (1988): Characterization of the proteins purified with monoclonal antibodies to glutamic acid decarboxylase. *J Neurosci* 8:2123-2130.

9. Fish KN, Sweet RA, Lewis DA (2011): Differential distribution of proteins regulating GABA synthesis and reuptake in axon boutons of subpopulations of cortical interneurons. *Cereb Cortex* 21:2450-60.

10. Hagiwara A, Fukazawa Y, Deguchi-Tawarada M, Ohtsuka T, Shigemoto R (2005): Differential distribution of release-related proteins in the hippocampal CA3 area as revealed by freeze-fracture replica labeling. *J Comp Neurol* 489:195-216.

11. Marty S, Wehrle R, Fritschy JM, Sotelo C (2004): Quantitative effects produced by modifications of neuronal activity on the size of GABAA receptor clusters in hippocampal slice cultures. *Eur J Neurosci* 20:427-440.

12. Fish KN, Sweet RA, Deo AJ, Lewis DA (2008): An automated segmentation methodology for quantifying immunoreactive puncta number and fluorescence intensity in tissue sections. *Brain Res* 1240:62-72.

13. Baddeley A, Vedel Jensen EB (2005): *Stereology for Statisticians.* Boca Raton, FL: Chapman & Hall/CRC.

14. Gundersen HJG (1977): Notes on the estimation of the numerical density of arbitrary profiles: The edge effect. *J Microsc* 111: 219–223.

15. Dorph-Petersen K-A, Nyengaard JR, Gundersen HJ (2001): Tissue shrinkage and unbiased stereological estimation of particle number and size. *J Microsc* 204:232-246.

16. Dorph-Petersen K-A, Caric D, Saghafi R, Zhang W, Sampson AR, Lewis DA (2009): Volume and neuron number of the lateral geniculate nucleus in schizophrenia and mood disorders. *Acta Neuropathol* 117: 369–384.

17. Sweet RA, Henteleff RA, Zhang W, Sampson AR, Lewis DA (2009): Reduced dendritic spine density in auditory cortex of subjects with schizophrenia. *Neuropsychopharmacology* 34:374-389.

18. Mijnster MJ, Galis-de-Graaf Y, Voorn P (1998): Serotonergic regulation of neuropeptide and glutamic acid decarboxylase mRNA levels in the rat striatum and globus pallidus: studies with fluoxetine and DOI. *Brain Res Mol Brain Res* 54: 64-73.

19. Costa E, Guidotti A (1979): Recent studies on the mechanism whereby benzodiazepines facilitate GABA-ergic transmission. *Adv Exp Med Biol* 123:371-378.

20. Treiman DM (2001): GABAergic mechanisms in epilepsy. *Epilepsia* 42 Suppl 3:8-12.

21. Izzo E, Auta J, Impagnatiello F, Pesold C, Guidotti A, Costa E (2001): Glutamic acid decarboxylase and glutamate receptor changes during tolerance and dependence to benzodiazepines. *Proc Natl Acad Sci U S A* 98:3483-3488.